J. Fluid Mech. (2001), *vol.* 443, *pp.* 329–350. Printed in the United Kingdom

Instabilities of the flow between a rotating and a stationary disk

By L. SCHOUVEILER, P. LE GAL AND M. P. CHAUVE

Institut de Recherche sur les Phénomènes Hors Equilibre,
UMR 6594 Universités d'Aix-Marseille I & II – CNRS, Technopôle de Château-Gombert,
49 rue Frédéric Joliot Curie, BP 146, F-13384 Marseille cedex 13, France

(Received 17 July 2000 and in revised form 26 March 2001)

This experimental study is devoted to the description of the different patterns resulting from instabilities which appear in the flow between a rotating and a stationary disk enclosed by a stationary sidewall. With the help of visualizations we describe the different flow regimes as functions of two control parameters: the Reynolds number and the aspect ratio of the gap separating the disks, which are varied over large continuous ranges. Moreover, visualizations and ultrasonic anemometry lead to the description of the different instabilities and to the construction of a transition diagram that summarizes the domains of existence of the various patterns. Two different scenarios of transition are mainly followed by the flow. When the gap between the two disks is more than the thickness of the two disk boundary layers, circular and spiral waves destabilize the stationary disk boundary layer. Transition occurs in this case by the mixing of these waves. On the other hand, when the two boundary layers are merged, finite-size turbulent structures can appear. They consist of turbulent spots or turbulent spirals which invade the laminar domains as the Reynolds number of the flow is increased.

1. Introduction

Because of their practical and academic interest, the viscous flows confined between rotating and stationary parallel disks have motivated numerous experimental, numerical and theoretical studies during the 20th century. Such flows can model situations encountered in geophysics and in many industrial applications such as turbomachinery (see e.g. the review by Owen & Rogers 1989). From a fundamental point of view, the research has been motivated in large part by the fact that for infinite geometries, exact similarity solutions of Navier–Stokes equations can be obtained for the stationary axisymmetric basic flow. They were first calculated by von Kármán in 1921 for the flow induced by a infinite disk rotating in a quiescent fluid and then generalized by Batchelor (1951) for the one- and two-disk flow families, the latter including the case where only one disk rotates. These similarity solutions allow the reduction of the Navier–Stokes equations to a system of ordinary differential equations. The solutions of these equations, and their multiplicity, have given rise to a large quantity of numerical work which has been the subject of a review by Zandbergen & Dijkstra (1987). Among these solutions, the one usually referred to as the Batchelor solution is of special interest. Batchelor (1951) conjectured that for large enough Reynolds number $Re_h = \Omega h^2/\nu$ (where Ω is the angular velocity of the rotating disk, h the axial distance between the two disks and ν the kinematic viscosity of the fluid)

the viscous effects are confined to boundary layers on each disk, separated by an inviscid core approximately in solid-body rotation with an angular velocity $\Omega_c = \beta\Omega$. Later, the constant entrainment coefficient β was calculated to be nearly equal to $1/3$ (Lance & Rogers 1962). When the Reynolds number Re_h is decreased, the Batchelor stationary flow with separated boundary layers evolves towards a purely viscous flow with merged boundary layers as obtained in the numerical study of Lance & Rogers (1962). An asymptotic analysis (see e.g. Schouveiler 1998) shows that the similarity solution tends towards a torsional Couette flow, with a linear azimuthal velocity profile, when Re_h tends towards zero.

Numerous experimental (e.g. Gauthier, Gondret & Rabaud 1999) and numerical (such as Dijkstra & van Heijst 1983) studies have shown that, for large enough Reynolds numbers, this Batchelor solution is at least qualitatively relevant for the finite configurations of the flows between a rotating and a stationary disk enclosed by a cylindrical sidewall. But for these finite geometries, the angular velocity of the core is a function of the radial coordinate, contrary to the Batchelor infinite disk flow, and therefore the flow deviates from the self-similar solution. However, just as in the infinite geometry, for decreasing Reynolds numbers Re_h the flow evolves towards a viscous torsional Couette flow (Sirivat 1991).

A considerable amount of research has been devoted to the stability of the one-disk flow family. In particular, these boundary layer flows of a rotating fluid (at the angular velocity Ω_f) above a rotating disk (at the angular velocity Ω) appear as a model for the stability study of three-dimensional boundary layers. Linear stability analyses of the similarity solutions have been performed by Faller (1991), Pikhtov & Smirnov (1993) and Lingwood (1997) over a wide range of the parameters Ω_f and Ω, including the three limiting cases ($\Omega_f = 0$, $\Omega \neq 0$), ($\Omega_f \neq 0$, $\Omega = 0$) and ($\Omega_f \approx \Omega$) respectively referred to as the von Kármán, Bödewadt (1940) and Ekman (1905) layers. These analyses, which have been conducted locally at the radial location r, have reported a characteristic two-lobe marginal surface. The two lobes are associated with two instabilities typical of the one-disk flows and are referred to as type 1 and 2 (according to the terminology introduced by Faller & Kaylor 1966*a*), and sometimes as class B and A (Greenspan 1968). The global minimum of the marginal surface corresponds to the type 2 (class A) instability. Both instabilities appear in the form of regular systems of spiral rolls confined to the disk boundary layer, but these roll-like patterns differ in orientation, phase velocity and wavelength.

Type 1 instability was first noticed in the von Kármán layer by Smith (1946), then by Gregory & Walker (see Gregory, Stuart & Walker 1955), and by Faller (1963) in the Ekman layer. Stuart (in Gregory *et al.* 1955) showed that type 1 instability results from an inviscid mechanism due to unstable inflection points in boundary layer velocity profiles. In spite of numerous experimental studies (e.g. Kobayashi, Kohama & Takamadate 1980; Wilkinson & Malik 1983), and although the stability analyses (Kobayashi *et al.* 1980; Balakumar & Malik 1990) predict that the most unstable type 1 modes have non-zero frequency relatively to the disk, experimental investigation of such travelling modes is fairly recent (Jarre, Le Gal & Chauve 1996).

Theoretical studies of Ekman layer stability by Lilly (1966) and Faller & Kaylor (1966*b*) have indicated the existence of the second (type 2) instability associated with the Coriolis terms, which appears to be dominant at low Reynolds numbers and stable in the non-viscous limit. These waves were first experimentally reported in the Ekman flow by Faller (1963) and in the von Kármán layer by Faller & Kaylor (1966*a*).

Owing to the difficulty of realizing experimentally a fluid flow in solid-body rotation

above a stationary disk, the stability of the Bödewadt boundary layer has been far less studied. Savas (1983, 1987) has performed transient spin-down experiments to approximate such a configuration. He has reported two different instabilities in the form of circular and spiral rolls which could correspond respectively to the type 2 and 1 instabilities (Pikhtov & Smirnov 1993). These observations have been confirmed by the experimental and computational investigations of Lopez (1996) and Lopez & Weidman (1996). From their extensive stability analysis, Pikhtov & Smirnov (1993) have concluded that the Bödewadt layer is the most unstable configuration of the one-disk flow family in agreement with the previously cited studies. Lingwood (1995, 1997) has also theoretically shown, and experimentally confirmed for the von Kármán flow (Lingwood 1996), that these one-disk flows are subject to an absolute instability whose onset is consistent with the onset of the transition to turbulence. Finally, a recent work (Fernandez-Feria 2000) presented a spatial linear stability analysis of the Bödewadt boundary layer. Some of these results will be compared later on to our own measurements.

The problem addressed in this paper is the stability of the flows confined between a rotating and a stationary disk. It has been far less studied than the stability of the one-disk flow family. To our knowledge the first publication exclusively devoted to this subject is by Wimmer (1978) who experimentally exhibited an instability mode appearing as a spiral roll system. Earlier, Daily & Nece (1960) had distinguished experimentally two types of laminar–turbulent transition when the angular velocity of the rotating disk is increased. Thus, according to the distance separating the two parallel disks, the transition can affect either the torsional Couette flow or the Batchelor flow. But these authors did not study the transition in great detail.

As pointed out by Zandbergen & Dijkstra (1987), the existence in a certain range of parameters of a rotating core (as described by the separated boundary layer Batchelor flow) provides a connection between the one- and two-disk flow families by considering $\Omega_f = \Omega_c$ and the angular velocity of the disk equal to 0 or Ω. For this case, the linear stability analysis of the similarity Batchelor solution has been performed by Itoh (1991) for the separated boundary layer regime and San'kov & Smirnov (1992) from separated to merged boundary layers. In parallel with these stability studies, experiments revealed the existence of various sequences of transition from the laminar basic regime to turbulent flow when one increases the Reynolds number, according to the value of the aspect ratio h/R.

In particular, in the case of separated boundary layers, it was found that the stationary disk boundary layer is the first to be destabilized by circular waves which propagate inwards (Schouveiler *et al.* 1996). These waves, which appear to be of the same type (apparently recognized as a type 2 instability by San'kov & Smirnov 1992) as the circular waves observed by Savas (1987) in his transient experiments, were also observed in numerical simulations (Lopez & Weidman 1996; Cousin-Rittemard, Daube & Le Quere 1998; Serre, Crespo Del Arco & Bontoux 2001). They were also particularly well characterized in the experimental study of Gauthier *et al.* (1999) who showed the convective nature of the instability. At higher values of the Reynolds number, another unstable mode has also been observed (Itoh 1988; Schouveiler *et al.* 1996; Serre *et al.* 2001). This secondary instability creates a spiral pattern which co-exists with the previous circular waves. The stability of this spiral wave pattern was then studied and the wavenumber selection process was described as a result of the Eckhaus instability (Schouveiler, Le Gal & Chauve 1998).

In the case of merged boundary layers, other instabilities were discovered by San'kov & Smirnov (1985), Itoh (1988) and Sirivat (1991). These instabilities are

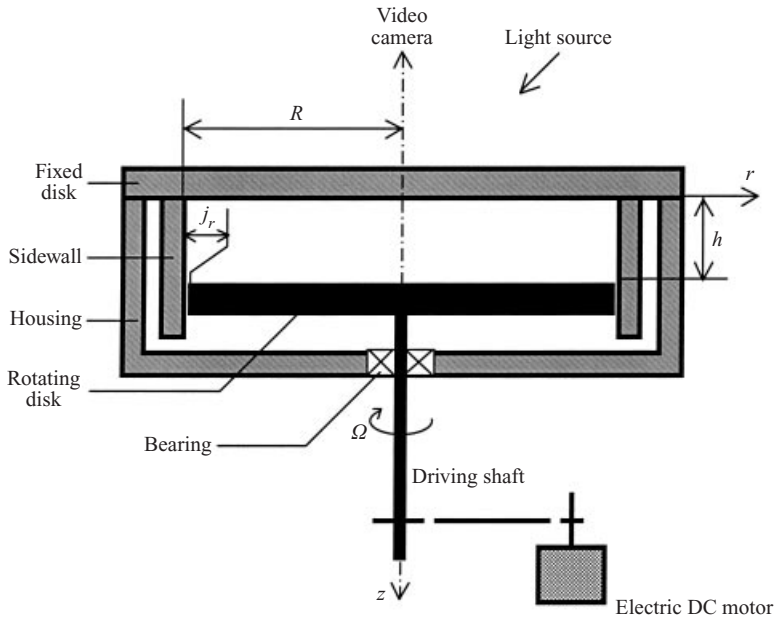

FIGURE 1. Experimental device. The radial gap j_r between rotating disk and sidewall is less than 0.05 mm.

mainly characterized by localized turbulent structures which can take the form of spots or of solitary waves (San'kov & Smirnov 1985). The number of these structures, which are usually superimposed on a short-wavelength spiral pattern, increases with the Reynolds number. A scenario of transition which may be related to the spatio-temporal intermittency scenario (Manneville 1991) leads finally to a completely turbulent flow.

This paper is organized as follows: § 2 is devoted to the description of our experimental setup. A summary of the different flow patterns visualized at large, intermediate and small aspect ratios is presented in an experimental transition diagram in § 3. Then, the flow regimes are characterized in §§ 4 and 5 using ultrasonic Doppler anemometry and flow visualizations. Before concluding (§ 7), the influence of the geometry is briefly discussed in § 6.

2. Experimental details

2.1. *Experimental apparatus*

The flow is confined in the gap between two horizontal coaxial parallel disks, one stationary and the other rotating at an adjustable speed. It is enclosed at the periphery by a stationary cylindrical sidewall. The experimental apparatus, schematically presented in figure 1, consists of a rotating disk made of stainless steel and of radius $R = 140$ mm, which can be driven in rotation by an electric DC motor. The variation of the rotational frequency N is obtained by varying the supply voltage of the motor. This frequency N, measured using an optical encoder (360 impulses/rev), can be varied continuously up to 2 Hz (2 r.p.s.). It is controlled with an accuracy of 0.01 Hz. Because of the difficulty of maintaining a stable angular velocity for the weakest rotation frequencies, no measurements were carried out for values of N lower than 0.1 Hz.

The disk is placed inside a stationary vertical cylindrical housing of circular interior section of 150 mm in radius and 60 mm in depth. The upper face of the housing is closed by a removable cover that constitutes the stationary disk. In order to ensure conditions of closed flow, the gap between the two disks is enclosed by a vertical cylindrical sidewall attached to the stationary cover. The radial distance j_r between the edge of the disk and the sidewall has been reduced to less than 0.05 mm, so that the rotation of the disk takes place without friction. The housing, the stationary disk and the sidewall are made entirely of Plexiglas to allow the flow visualizations and ultrasonic measurements of the velocity.

The housing is completely filled with water at ambient temperature. The experiments were realized at a constant ambient temperature of 20 °C, to within ± 1 °C, so that the kinematic viscosity of the working fluid is $\nu \approx 1\,\mathrm{mm^2\,s^{-1}}$. The draining and filling operations of the housing are carried out through two openings in the cover and in the bottom plugged during the experiments.

A device with a ball thrust allows the vertical displacement of the rotating disk in such a way that the axial distance h between the two disks can be adjusted continuously up to 20 mm with an accuracy better than 0.02 mm. Geometric imperfections including the flatness and roughness defects were measured to induce a variation of the height h of less than 0.07 mm. The experimental results presented in this paper were realized for values of h of more than 1 mm in order to limit the relative inaccuracy in the distance h.

The two experimental parameters are the rotation frequency N (or the angular velocity of the rotating disk $\Omega = 2\pi N$), and the axial distance h separating the two disks. For comparisons with previous studies, in particular with stability analyses, we have chosen R and Ω^{-1} as characteristic scales of length and time respectively, so that the flow control parameters are the Reynolds number $Re = \Omega R^2/\nu = Re_h(h/R)^{-2}$ and the aspect ratio h/R. Finally, we define a cylindrical coordinate system (r, θ, z) fixed to the stationary disk (laboratory frame), with origin at the centre of the stationary disk and with the z-axis pointed towards the rotating disk (figure 1).

Two other geometries, presented in figure 2, have been used to investigate the influence of the radial boundary conditions. The first one, shown in figure 2(*a*), is obtained by removing the vertical sidewall from the cover. In this case, there is a radial gap j_r equal to 10 mm between the rotating disk and the housing. The second geometrical configuration (figure 2*b*) is realized by adding to the stationary cover a vertical shroud which has an inner radius of 130 mm. An axial gap j_a of 1 mm separates the rotating disk from this stationary cylinder. We will see in § 6 the strong influence of the boundary conditions on the pattern selection.

2.2. *Investigation techniques*

The hydrodynamic structures which develop in the flow during its transition from laminar to turbulent states are visualized by a classical method using reflective anisotropic particles in suspension in the flow. This method was quantitatively analysed by Savas (1985) and more recently by Gauthier, Gondret & Rabaud (1998). The flow is seeded with flake particles which have a typical length of less than 15 μm and a density at 20 °C of about $3\,\mathrm{g\,cm^{-3}}$. They consist of mineral mica platelets coated with metal oxide (oxide of tin and titanium dioxide) which provides them with a strong index of reflection of light. Although their movement is rather complex (Gauthier *et al.* 1998), our previous experiments (Schouveiler 1998; Schouveiler *et al.* 1999) have shown, by comparisons of visualizations and velocity measurements, that under suitable conditions of lighting these particles are good tracers of the hydrodynamic structures.

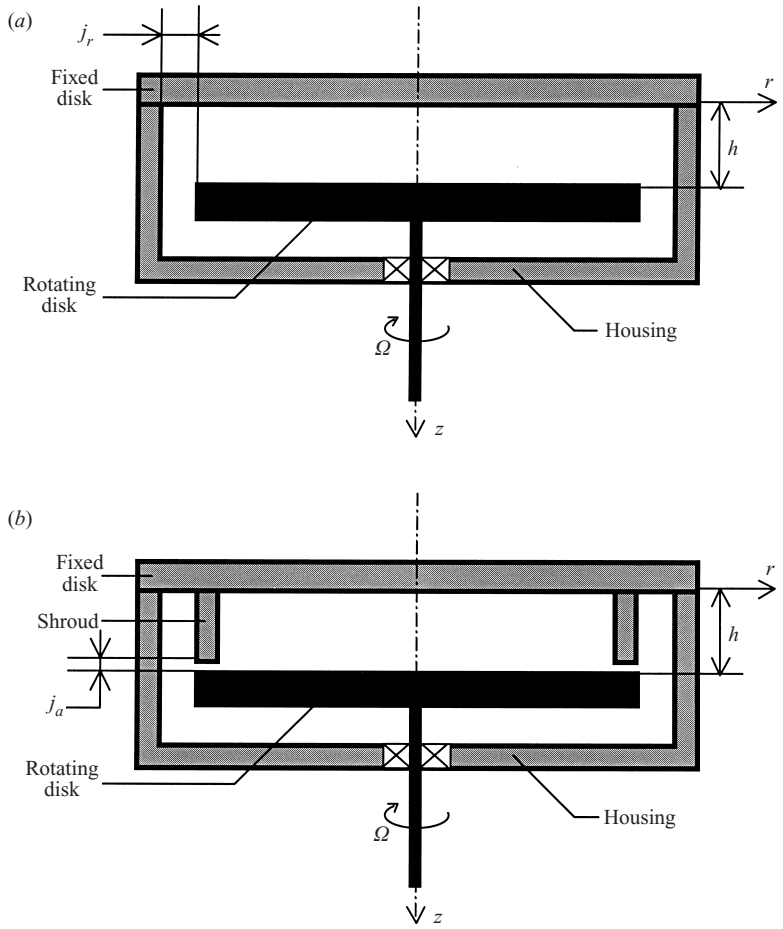

FIGURE 2. The two different disk and boundary configurations: (*a*) geometry with radial gap $j_r = 10\,\text{mm}$, (*b*) geometry with axial gap $j_a = 1\,\text{mm}$.

Their slow sedimentation permits the flow pattern to be visualized for several hours. Note that we have not taken into account the variation of the kinematic viscosity of the fluid due to the presence of the small amount of these particles. The flow is illuminated with a 1000 W projector of white light inclined with respect to the rotation axis (figure 1). This non axisymmetric lighting induces a slight apparent inhomogeneity in the visualizations.

The flow patterns are visualized through the fixed disk and for all the flow images presented, the rotating disk turns in the clockwise direction. The light scattered by the particles is captured, at the video frequency of 25 images per second, by means of a black and white camera placed on the rotation axis (see figure 1) and fixed in the laboratory frame (i.e. stationary disk). The images are recorded on standard videotape and can be digitized, on 512×512 pixels, with an image processing board controlled by a microcomputer. Each pixel is coded on a grey scale ranging between 0 (black) to 255 (white). The digitized images can then be processed. In particular, space–time images are built-up by a sequential accumulation of video lines, taken on a radius of the disk, at standard video rate (25 Hz). Such images provide information on the spatio-temporal dynamics of the observed structures.

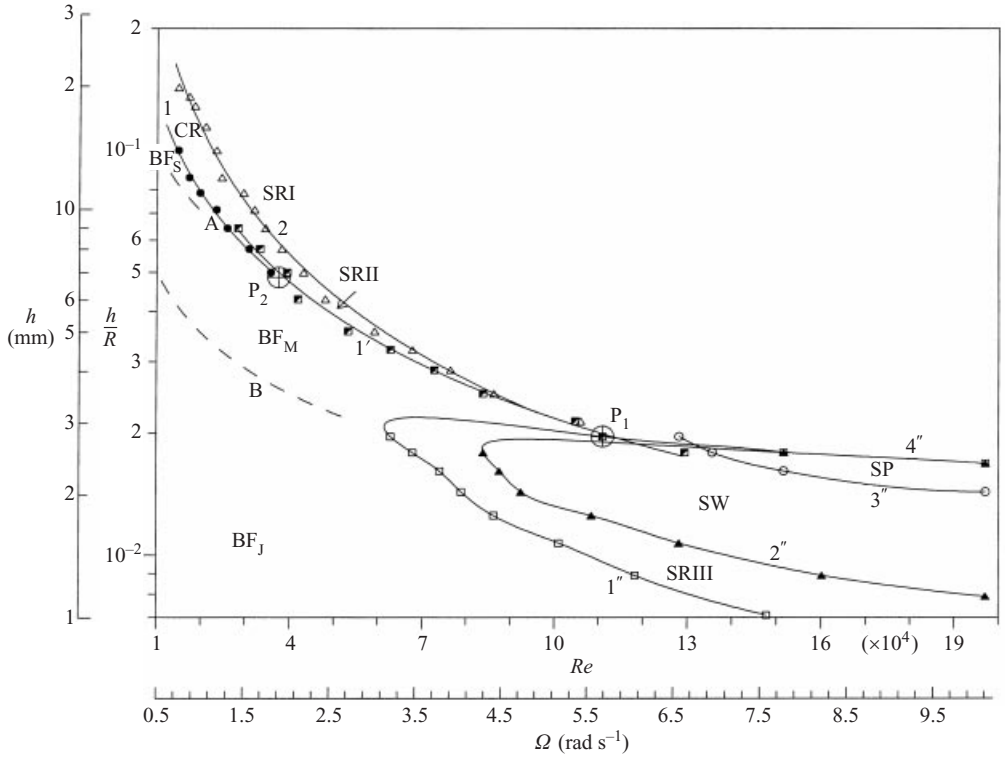

FIGURE 3. Transition diagram of the flow between a rotating and a stationary disk enclosed by a stationary sidewall. Curves A and B separate the mixed basic flow (BF_M) from the basic flows with separated boundary layers (BF_S) and with joined boundary layers (BF_J) respectively. Curves 1 and 2 are the thresholds for the circular rolls (CR) and the spiral rolls (SRI) respectively. Curve 1′ is the spiral roll (SRII) threshold. Curves 1″, 2″ and 3″ are the thresholds for the spiral rolls (SRIII), the solitary waves (SW) and the spots (SP) respectively. Curve 4″ is the threshold for the simultaneous disappearing of the spiral rolls (SRIII) and of the solitary waves (SW). These thresholds have been determined by increasing the Reynolds number *Re*, hysteresis cycles have been demonstrated for the thresholds 2″ and 4″.

Complementary information has been obtained by using an ultrasonic Doppler velocimeter working with a pulsed ultrasonic emission. For this, the flow was seeded with nylon spherical micro particles (80 μm in diameter, and of density 1.02 g cm^{-3}). By detecting the Doppler frequency shift of ultrasonic pulses reflected by the particles, this device allows measurement of temporal series of instantaneous profiles, along the ultrasound beam, of the velocity component in this direction. This technique has been presented in detail by Takeda (1986). Unlike visualizations, these measurements provide information about the axial structure of the flow.

3. Experimental procedure and transition diagram

The principal result of this experimental study is the transition diagram shown in figure 3. It is obtained by a systematic exploration (following the procedure described below) of the portion of the control parameter space ($h/R, Re$) accessible with our apparatus. This exploration has been done to identify the various flow regimes, which

are denoted with initials in figure 3. To determine the stability domains of these regimes, the distance h was fixed and the rotation frequency N increased slowly (quasi-statically) from 0 to 2 r.p.s. After each variation of N, we waited long enough for the asymptotic regime of the flow to be reached. This time delay, from ten minutes to about one hour, was always much larger than the spin-up time of the flow defined as the quadratic average of inertial and viscous times (Greenspan 1968). Then N was decreased back in the same manner to check the existence of possible hysteresis cycles. This procedure was repeated for numerous values of h between 1 and 20 mm. The reproducibility of the results was verified by conducting several experimental runs.

Curves 1 to 4″ in figure 3 were obtained by interpolating the experimental points which correspond to transition boundaries between flow regimes. These transitions have been established by visual observations for increasing N. As all the instabilities are first observed at the periphery of the disk, we will use the Reynolds number $Re = \Omega R^2/\nu$ which corresponds to the value at $r = R$ of a local Reynolds number based on r. As discussed in the next sections, hysteretic features have been observed only for boundaries 2″ and 4″. The determination of these bifurcation thresholds from one state to another depends on the sensitivity of the visualization technique, which tends to slightly overestimate these values because the structures become observable only when they have reached a large enough amplitude.

As reported in previous studies (see § 1), some of the flow regimes (denoted CR and SR in figure 3) result from the development of instabilities that generate regular roll-like patterns. These roll systems appear on the visualizations as alternate clear and dark bands forming spirals or circles around the disk axis. Because the angle ε between the spiral axis and the tangential direction does not present a noticeable variation along a radius, they can be approximated by logarithmic spirals. According to the usual convention, the angle ε is counted positive when spirals are rolled up towards the disk axis in the rotation sense of the rotating disk. The roll-like patterns are thus characterized by the orientation angle ε and the local (along the radius r) quantities such as the wavelength λ or the number n of structures present on the circumference r. These quantities are related by the approximate relation (by neglecting the curvature of the circumference over one wavelength): $\lambda = (2\pi r/n)\sin\varepsilon$. For all the instabilities, the temporal dependence is discussed relative to the reference frame with respect to the fixed disk, i.e. to the laboratory frame. Frequencies f (possibly functions of r) are deduced from Fourier transforms either of space–time images (see § 2.2) or of ultrasonic Doppler measurements of radial velocity profiles along a radius as presented in Schouveiler *et al.* (1999).

Itoh (1988) and San'kov & Smirnov (1985) have also presented experimental transition diagrams for a similar system of enclosed flow between a stationary and a rotating disk, but the former considered only five values of the aspect ratio h/R between 0.80×10^{-2} and 12.0×10^{-2}, and the latter had a restricted range of this parameter (i.e. $0.67 \times 10^{-2} \leqslant h/R \leqslant 6.33 \times 10^{-2}$). In the present work, the variation of the experimental parameters h between 1 and 20 mm and N from 0 to 2 r.p.s. corresponds to exploration ranges for the two control parameters h/R and Re of, respectively $[0.71 \times 10^{-2}, 14.28 \times 10^{-2}]$ and $[0, 246.3 \times 10^{3}]$. We will see that our observations are in good agreement with these previous investigations.

The transition diagram (figure 3) is represented simultaneously in the (h, Ω) plane and in the $(h/R, Re)$ plane. It reveals a large variety of flow regimes which are denoted by initials: BF for basic flow, CR for circular rolls, SR for spiral rolls, SW for solitary waves and SP for spots. These different patterns are described in the next sections.

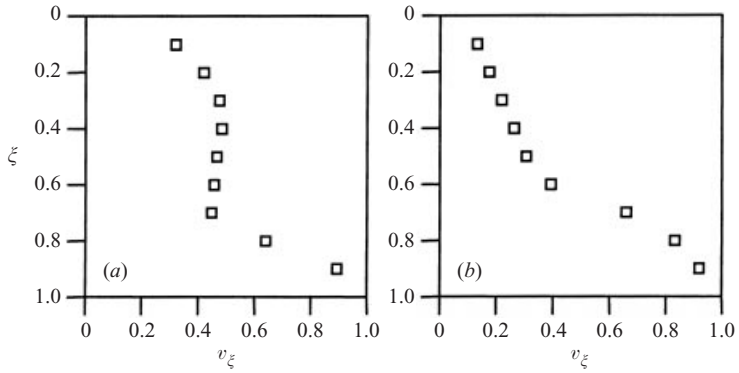

FIGURE 4. Typical mean velocity profiles $v_\xi(\xi)$ measured by ultrasonic Doppler velocimetry for $h/R = 5.0 \times 10^{-2}$: (*a*) separated boundary layers: $r/R = 0.85$, $Re = 36.9 \times 10^3$ ($Re_h = 92.36$) and (*b*) joined boundary layers: $r/R = 0.357$, $Re = 18.5 \times 10^3$ ($Re_h = 46.18$).

4. Basic regimes

At very low Reynolds number Re and for all the explored values of the aspect ratio h/R, the flow appears stationary and axisymmetric. The region of stability of this basic flow corresponds to three areas denoted by BF in figure 3. It is limited at high Re by the curves 1, 1′ and 1″. It is not our intention here to provide a complete description of this well-known basic flow (see § 1) but just to recall few characteristic results. Our measurements confirm previous studies showing that the basic regime is a Batchelor-type flow which evolves from a purely viscous flow to a flow with separated boundary layers as Re_h is increased. We studied the velocity field of this basic flow by ultrasonic Doppler anemometry at various radius location and for various values of the flow parameters. The ultrasound beam passes through the cover and is confined to an azimuthal plane (at a chosen radius r). It is directed along a local ξ-axis which makes an angle of $\alpha = 20°$ with the vertical axis. This value of 20° is a good compromise to minimize the echoes and reflections of the ultrasound beam (see details in Schouveiler *et al.* 1999). Although the mean velocity profiles $v_\xi(r, \xi)$ obtained in this way are combinations of the three components of the velocity, they distinguish the nature of the mean flow between Batchelor-type flow with separated boundary layers and the torsional Couette flow with merged boundary layers. Velocity v_ξ is non-dimensionalized by $r\Omega \sin\alpha$ and the ξ-coordinate is chosen to be 0 on the fixed disk and 1 on the rotating one.

For large Re_h, the non-dimensional mean velocity profile $v_\xi(\xi)$ presents the same characteristics as the azimuthal velocity profile of the Batchelor-type flow (see figure 4(*a*), where $Re_h = 92.36$). It is possible to distinguish a boundary layer on the fixed disk and one on the rotating disk (respectively at $\xi < 0.3$ and $\xi > 0.7$). These two layers are separated by an inviscid rotating core ($0.3 < \xi < 0.7$) in which the velocity gradient is weak. As mentioned in previous experimental studies, one can see that, as Re_h is decreased, the flow evolves to a purely viscous flow. As can be seen in figure 4(*b*) for $Re_h = 46.18$ the boundary layers which develop on each disk are joined.

By measuring mean velocity profiles $v_\xi(\xi)$ at various radii we found also that, over a certain range of the experimental parameters, the basic flows have boundary layers joined up to a certain radius and separated beyond. In agreement with numerical simulations of Randriamampianina *et al.* (1997), we observe that this non-viscous

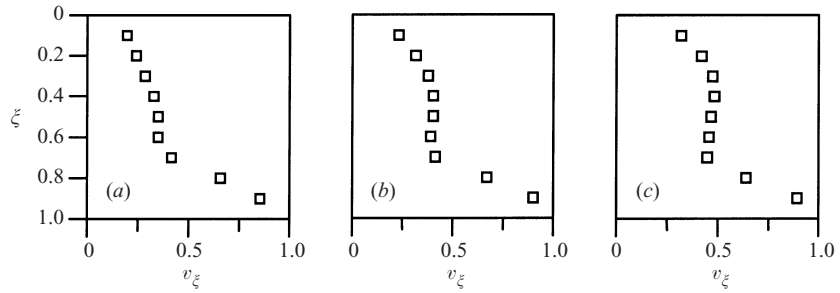

FIGURE 5. Evolution of mean velocity profile $v_\xi(\xi)$ with the radius r in the case of mixed basic flow (BF_M) for $h/R = 5.0 \times 10^{-2}$, $Re = 36.9 \times 10^3$ ($Re_h = 92.36$). (*a*) $r/R = 0.357$, (*b*) $r/R = 0.643$, (*c*) $r/R = 0.850$.

part of the flow starts to be formed close to the periphery before extending towards the centre, when increasing the Reynolds number. As presented in figure 5, for some experimental configurations, the velocity profiles $v_\xi(\xi)$ measured at various radii reveal that the thickness of the boundary layers on both disks varies so that the rotating core occupies an increasing proportion of axial space as r is increased, as observed by Gauthier *et al.* (1999). This result is also in agreement with previous studies (Dijkstra & van Heijst 1983) which show that this radial evolution results from the increase of the angular velocity $\Omega_c = \beta\Omega$ of the rotating core with r. We have mentioned that the nature of the velocity $v_\xi(\xi)$ makes any quantitative analysis difficult, but, since the radial and axial velocities of the Batchelor flow are small in the rotating core, we can obtain an estimated angular velocity of the central part by using the velocity measurements $v_\xi(\xi)$ at mid-height: $v_\xi(\xi = 0.5) \approx \Omega_c/\Omega = \beta$. In this way, for the situation presented in figure 5 ($Re = 36.9 \times 10^3$, $h/R = 5.0 \times 10^{-2}$) this angular velocity evolves from $\Omega_c = 0.35\Omega$ at $r/R = 0.357$, to $\Omega_c = 0.40\Omega$ at $r/R = 0.643$ and to $\Omega_c = 0.46\Omega$ at $r/R = 0.850$. These results overestimate the angular velocity of the rotating core since the axial velocity of the flow is not strictly zero in this area. Nevertheless, they are of same order as those of previous studies (Dijkstra & van Heijst 1983) where β has been found to be an increasing function of the radius.

In summary, when the Reynolds number Re_h increases, the viscous effects are increasingly confined to the vicinity of the two disks but this confinement is non-homogeneous along the radius. Therefore, we distinguish three types of basic flows whose regions of stability correspond to the three areas denoted BF_J, BF_M and BF_S respectively in figure 3. For the smallest values of Re_h, the basic flow appears to be purely viscous, i.e. the boundary layers which develop on each disk are joined over all the radial extent (the corresponding area is labelled BF_J). Then, at higher Re_h, a rotating core is formed close to the periphery. The flow is then in a mixed state (corresponding area denoted BF_M). The boundary layers are joined up to a certain radius and are separated beyond. When Re_h is increased still further, the rotating core extends towards the centre until it occupies the entire radial extent apart from close to the shroud at the periphery. The basic flow possesses two separated boundary layers (area called BF_S). The boundaries between these areas (dotted curves A and B in figure 3) are determined by measuring the velocity profiles v_ξ on a radius between $0.15 \leqslant r/R \leqslant 0.85$ and for various values of the parameters $(h/R, Re)$. In fact, a good approximation of curve A is simply given by $Re_h = 100$ and curve B by $Re_h = 25$. Thus, when $Re_h > 100$ (area denoted BF_S above curve A) the flow is always of Batchelor type with separated boundary layers over all the radial extent

($0.15 \leqslant r/R \leqslant 0.85$). These layers, whose thickness decreases with r, are separated by an inner core which rotates with a non-constant angular velocity Ω_c. In contrast, for $Re_h < 25$ (area called BF_J below curve B), the flow is always purely viscous, with joined boundary layers.

5. Secondary and subsequent regimes

When the Reynolds number Re is increased, we have observed different bifurcations of the flow starting from a critical threshold that depends strongly on h/R and thus on the type of basic flow. Our exploration reveals three distinct regions for which the primary bifurcation leads to the formation of three types of different patterns denoted (CR), (SRII) and (SRIII) on the transition diagram of figure 3. The limits of stability of the basic flow with respect to these new states are represented by the curves 1, 1′ and 1″. Secondary and subsequent flow regimes can then occur. Their domains of appearance are limited by curves noted 2, 2″, 3″ and 4″. The resulting flows are presented in the following sections according to the aspect ratio h/R.

5.1. *Large aspect ratio instabilities*

We present here the sequence of bifurcations observed for the highest values of the aspect ratio: $7.14 \times 10^{-2} \leqslant h/R \leqslant 14.29 \times 10^{-2}$ ($10\,\text{mm} \leqslant h \leqslant 20\,\text{mm}$). In this range, the basic flow loses its stability from a threshold Re_1, a function of h/R and represented by curve 1 on the transition diagram of figure 3. Along this boundary, the Reynolds number Re_h is always higher than 100, meaning that the transition affects a Batchelor-type flow with separated boundary layers (BF_S). Note that the experimental threshold is higher than that predicted by Fernandez-Feria (2000) in the linear spatial analysis of the Bödewadt boundary layer. The loss of stability of this basic mode leads to the formation of circular rolls (CR) ($\varepsilon = 0°$), similar to the waves observed by Savas (1983) in his transient experiments, centred on the axis of the disks and which appear at the periphery of the system and travel towards the centre. Their radial negative phase velocity evolves from $7\,\text{mm}\,\text{s}^{-1}$ at $r/R = 0.9$ to $5\,\text{mm}\,\text{s}^{-1}$ at $r/R = 0.4$ for example for $Re = 17.2 \times 10^3$ and $h/R = 11.43 \times 10^{-2}$. A visualization of these waves is presented in figure 6(*a*). As described by Schouveiler *et al.* (1999), the frequency associated with this instability is strongly correlated with the rotational frequency N of the rotating disk and varies radially. Following two successive roll pairings, it evolves from $3N$ at the periphery to N when the circular waves approach the centre. These frequencies are compatible with the values calculated by Fernandez-Feria (2000) which are close to the lower boundary of the unstable region as calculted in this analysis. The pairings or merging of these circular rolls can be seen on the space–time diagram constructed as described in § 2.2 and presented in figure 6(*b*). They are also reported in the numerical simulations of Cousin-Rittemard (1996) but not in the experiment by Gauthier *et al.* (1999). This process is not yet totally understood. The wavelength of these corotating circular rolls can be measured on the visualizations. We obtained a value around 15 mm which gives a dimensionless wavenumber, using the length scale $(\nu/\Omega)^{1/2}$, of 0.42 in complete agreement with the observations of Savas (1983) and with the calculation of Fernandez-Feria (2000). The double-hump structure of the eigenmode calculated by this analysis is similar to the profile we measured by ultrasound anemometry (Schouveiler *et al.* 1999). A precise description of this instability was also recently obtained (Gauthier *et al.* 1999), where it is shown that this circular wave instability is of convective type, leading to a high sensitivity to external controlled or uncontrolled forcing.

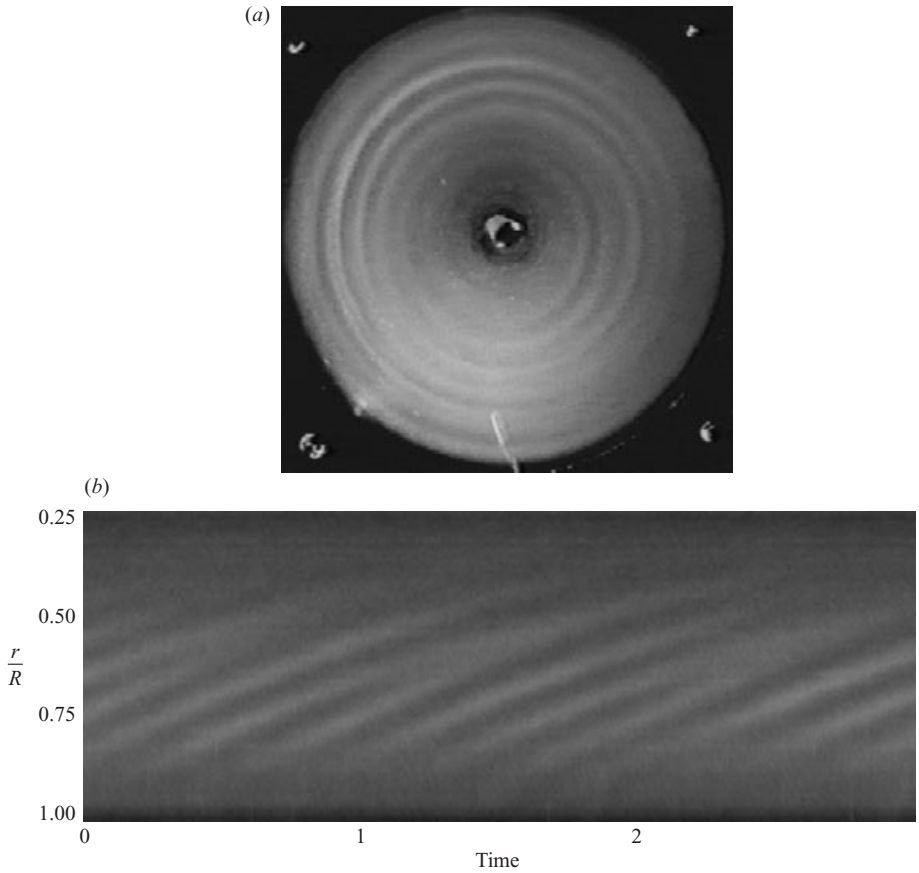

FIGURE 6. (*a*) Visualization of the circular rolls (CR) for $h/R = 11.43 \times 10^{-2}$, $Re = 17.2 \times 10^{3}$. (*b*) Corresponding space–time diagram showing the propagation of the circular rolls and their periodic pairings (dotted circles). Time is expressed in units of disk rotation period.

When increasing the Reynolds number, a second bifurcation is observed at a second threshold (curve 2 on figure 3). This bifurcation leads to the development of a system of spiral rolls (SRI) which appears in the peripheral region of the flow. The axisymmetry of the flow is thus broken by this second bifurcation. These spirals are defined by an angle ε of about 25° and coexist with the axisymmetric waves described previously. The visualization of figure 7 shows the coexistence of the spiral rolls (SRI) in the periphery of the system and the circular rolls (CR) in the central area. The spiral rolls are corotating and non-stationary both in the reference frame of the fixed disk and in the rotating disk frame. These waves, which result from a Hopf bifurcation (Schouveiler *et al.* 1998), progress outwards, i.e. with a positive radial phase velocity. A previous study was devoted to the Eckhaus secondary instability which selects the number of spiral arms (Schouveiler *et al.* 1998). At threshold, the number of rolls is 18, but depending on the initial conditions of the flow, states with 16 to 24 arms can be obtained. Unlike the circular waves, their frequency is not locked to the disk rotation frequency N and varies from 1.7 to 4 times N.

By the use of ultrasound anemometry, we have also already shown (Schouveiler *et al.* 1999) that both wave systems appear in the boundary layer of the stationary disk. These observations agree with stability analyses of San'kov & Smirnov (1992)

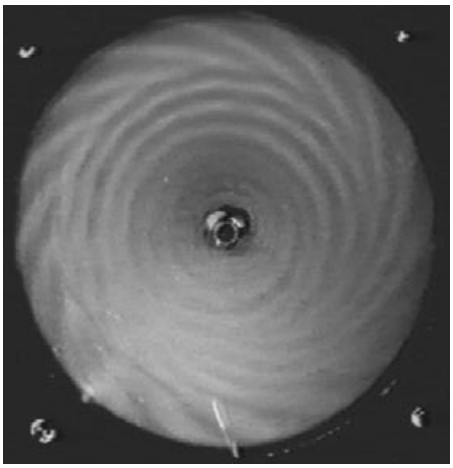

FIGURE 7. Visualization of the flow for $h/R = 11.43 \times 10^{-2}$, $Re = 20.9 \times 10^3$ showing the coexistence of the circular (CR) and spiral (SRI) rolls.

and Itoh (1991), which predict that the Bödewadt layer is the most unstable region of the flow. When the Reynolds number is further increased, the flow resulting from the coexistence of these modes of axisymmetric and spiral instability becomes increasingly complex without any apparent development of a new instability, as shown in the series of three space–time diagrams of figure 8. We can easily distinguish on these views the opposite propagation of the circular and of the spiral waves. As can be seen, 'wave turbulence' appears by interaction between the two kinds of waves (see figure 9) and has a characteristic granular appearance with a typical length given by the distance h.

5.2. *Small aspect ratio instabilities*

When $0.71 \times 10^{-2} \leqslant h/R \leqslant 1.79 \times 10^{-2}$ ($1\,\text{mm} \leqslant h \leqslant 2.5\,\text{mm}$), the process of transition is very different from that previously presented. In this case, the primary bifurcation occurs for values of Re_h lower than 25 and is thus associated with the destabilization of the purely viscous basic flow, i.e. with joined boundary layers (basic flow denoted BF_J). Daily & Nece (1960), for $h/R = 1.27 \times 10^{-2}$, and Sirivat (1991), for $h/R = 1.4 \times 10^{-2}$, also describe a primary bifurcation occurring for these small aspect ratio flows. Beyond a threshold represented by curve $1''$ on figure 3, this instability generates a network of spiral vorticies (SRIII) whose visualization is presented in figure 10(*a*). These spirals, also observed by Chauve & Tavera (1984), San'kov & Smirnov (1985), Itoh (1988) and Sirivat (1991), are defined by a small angle ε between $-3°$ and $-5°$. Their wavelength is of the order of the thickness h of the fluid layer and they propagate with a small radial phase velocity which can be positive or negative.

Above a second threshold Re_2'', which is also a function of h/R (curve $2''$ in figure 3), we observe the formation of turbulent stuctures having a spiral shape (SW). These spirals are more tilted (the angle ε is about $-20°$) and are superimposed on the SRIII network as shown on figure 10(*b*). These structures present neither spatial nor temporal periodicity. Each has its own dynamics and they rotate in the same direction as the disk but with a different angular velocity. For these reasons, San'kov & Smirnov (1985) use the terminology 'solitary waves' that we will retain here. A third type of structure, called spots (SP) because of their localized appearance (of the order of

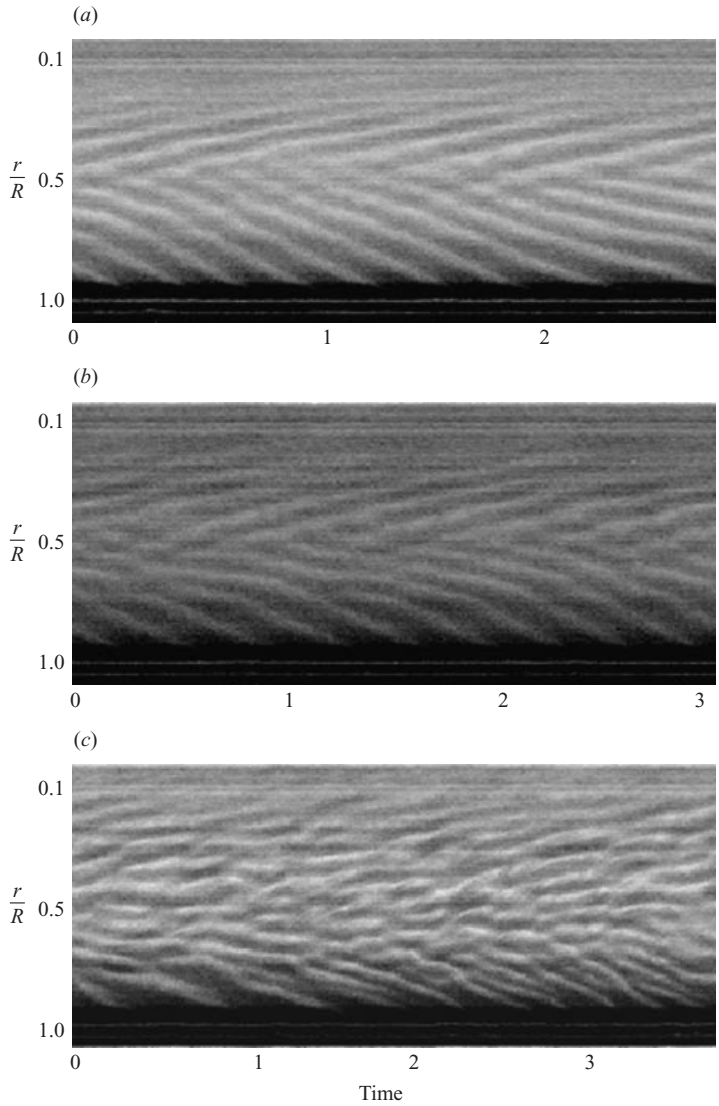

FIGURE 8. Space–time diagrams showing the transition to 'wave turbulence' for $h/R = 8.57 \times 10^{-2}$. (*a*) $Re = 33.3 \times 10^3$, (*b*) $Re = 36.9 \times 10^3$, (*c*) $Re = 46.6 \times 10^3$. Time is expressed in units of disk rotation period.

2 mm), appears above a third critical value Re_3'' (curve 3″ in figure 3). These spots are formed at the periphery of the container and move towards the centre on spiral trajectories while passing through the SRIII rolls and solitary waves. Some of these spots can be seen on figure 11(*a*). Finally, when Re exceeds a value Re_4'' (curve 4″) both the spiral structures and the solitary waves disappear. The spots penetrate further towards the centre and their number increases. The flow is then turbulent except in the central region as shown in figure 11(*b*). Figure 12 is a schematic bifurcation diagram which presents the succession of instabilities observed during the transition of torsional Couette flow (BF_J) to turbulence. Hysteresis cycles have been clearly demonstrated for the transition to the SW and SP regimes, as is classically the case

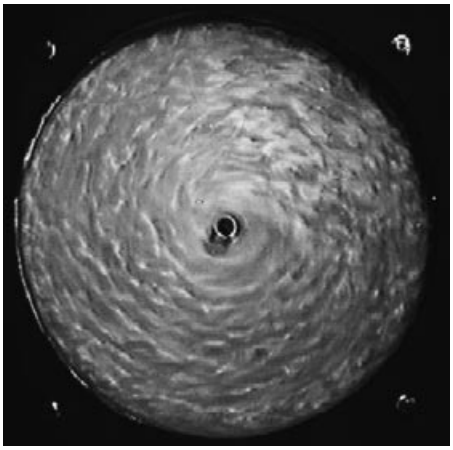

FIGURE 9. Visualization of the 'wave turbulence' regime for $h/R = 11.43 \times 10^{-2}$, $Re = 61.6 \times 10^3$.

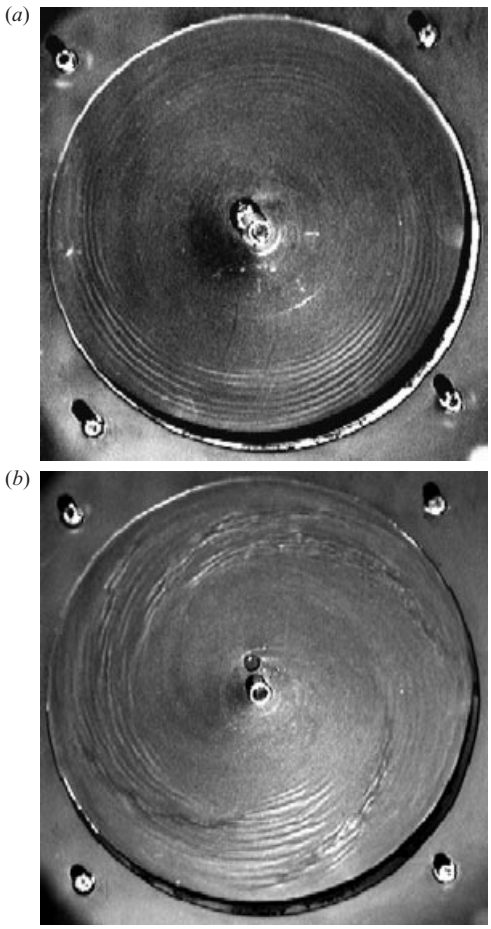

FIGURE 10. Visualizations of the flow for $h/R = 1.43 \times 10^{-2}$. (*a*) $Re = 89.9 \times 10^3$: spiral roll system (SRIII), (*b*) $Re = 126.8 \times 10^3$: coexistence of spiral rolls (SRIII) and solitary waves (SW).

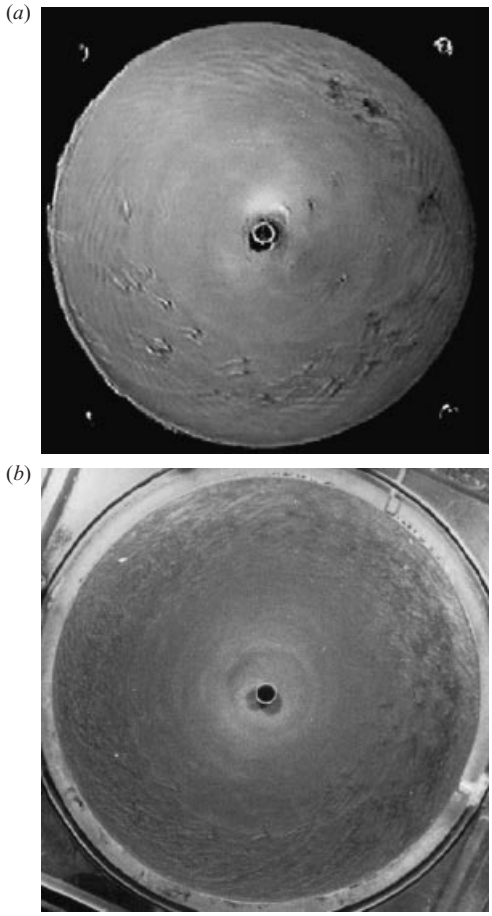

FIGURE 11. Visualization of the flow for $h/R = 1.96 \times 10^{-2}$. (*a*) $Re = 168.7 \times 10^3$: spots (SP), (*b*) $Re = 190.0 \times 10^3$: turbulence.

for the transition of plane Couette flow (Daviaud, Hegseth & Bergé 1992). Indeed the torsional Couette flow has a linear azimuthal velocity profile whose stability can be compared with that of plane Couette flow. For instance, the critical Reynolds number associated with the transition to the turbulent solitary waves (SW) and based on half the thickness h of the fluid layer, has a value around 340 which is close to the threshold given for the appearance of turbulent spots in plane Couette flow (Dauchot & Daviaud 1995).

5.3. *Intermediate aspect ratio instabilities*

For intermediate values of the aspect ratio h/R, i.e. between 1.79×10^{-2} and 7.14×10^{-2} ($2.5\,\text{mm} \leqslant h \leqslant 10\,\text{mm}$), only one mode of instability, which was not observed for the aspect ratio ranges previously presented, appears. This mode develops starting from a threshold Re_1' corresponding to curve 1′ and consists again of a network of spiral structures (denoted SRII, see figure 13) whose axes have a positive angle ε with the azimuthal direction; ε has been measured to be between 12° and 15° and the typical wavelength of this spiral pattern is given by the fluid layer thickness h. These spirals are stationary in the reference frame of the laboratory. This stationary network was observed in previous experimental studies (e.g. Wimmer 1978; Itoh 1988; Rabaud

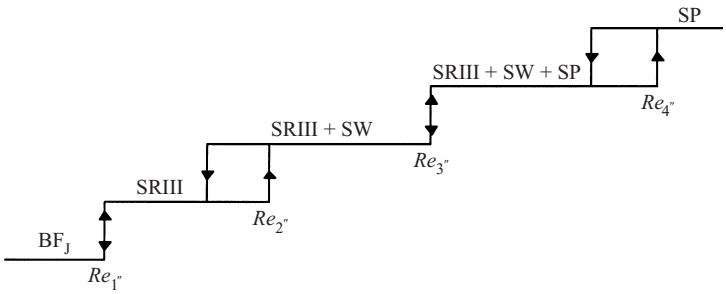

FIGURE 12. Schematic of the sequence of bifurcations for small aspect ratios.

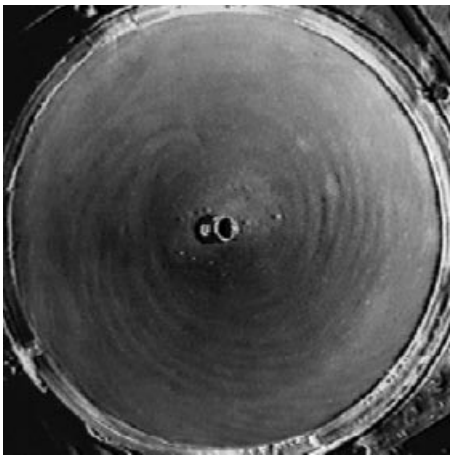

FIGURE 13. Visualization showing the existence of the stationary spiral rolls (SRII) for $h/R = 4.29 \times 10^{-2}$, $Re = 50.5 \times 10^3$.

1994), and the angle ε that we measure is consistent with these observations. Wimmer was the first to present a visualization of this system and to describe it as consisting of corotating rolls; San' kov & Smirnov (1984) note that it results from a supercritical bifurcation.

For these intermediate values of h/R, it is even possible to observe the superposition of three types of structures. When the critical value Re_1 is between the thresholds of formation of the circular roll network (denoted CR, curve 1) and of the SRI system (curve 2), the three systems of rolls (CR, SRI and SRII) coexist. Their dynamics can be oberved on the space–time image of figure 14. For $r/R > 0.7$, the inclined traces correspond to SRI rolls propagating radially outwards. In the area defined by $0.5 < r/R < 0.75$, one can distinguish the traces parallel with the time axis of the stationary rolls (SRII). Finally, the inclined traces observed for $r/R < 0.55$ are due to the propagation of the circular rolls (CR).

The complexity of the flow is also illustrated by the presence of two points (P_1 and P_2 in figure 3) of codimension greater than 1. These are intersections of stability curves of different modes. This was also recognized by Hoffmann, Busse & Chen (1998) and is often associated with a chaotic competition between patterns but we have not observed this. In P_1 the spiral rolls SRI, SRII and SRIII are destabilized together and in P_2, the circular rolls CR can appear simultaneously with the SRII spiral rolls.

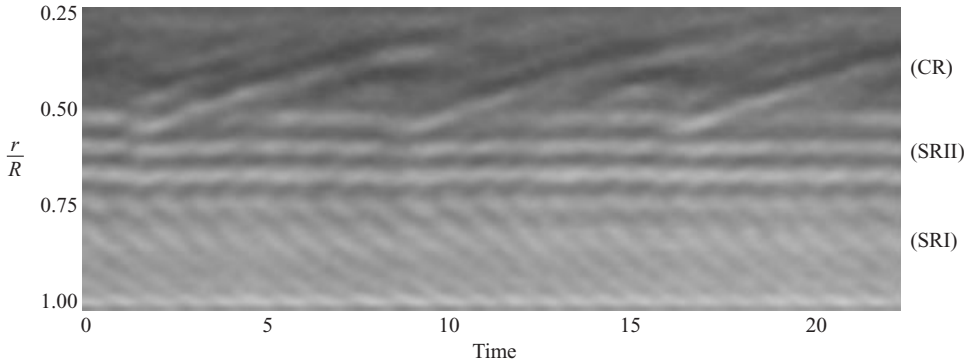

FIGURE 14. Space–time image ($h/R = 5.0 \times 10^{-2}$, $Re = 46.8 \times 10^3$) showing the coexistence of the outward travelling spiral rolls (SRI), stationary spiral rolls (SRII) and inward travelling cicular rolls (CR). Time is expressed in units of disk rotation period.

6. Influence of the geometry

Comparison between the transition processes described in § 5 and those reported in previous experimental work shows globally a good agreement. However we noted two differences. The first one concerns the fact that Wimmer (1978) and Itoh (1988) mention the existence of network SRII for values of the aspect ratio higher than those where we observe it (i.e. higher than 6.43×10^{-2}). The second difference is an instability which we did not observe in our system, but which was visualized by Sirivat (1991) for aspect ratios $h/R = 2.25 \times 10^{-2}$ and 4.75×10^{-2}, and consists of a system of stationary and quasi-circular rolls ($\varepsilon \approx 0°$). We think that the differences in the boundary conditions are the origin of this discrepancy. Indeed, the devices used by Wimmer and Itoh have a radial gap j_r, see figure 2(*a*), of about 0.5% of the radius R of the disk for the former and 0.8% for the latter, whereas in our case j_r is lower than 0.04% of R. The device used by Sirivat has an axial gap j_a as presented in figure 2(*b*). This gap accounts for 17.5% of the total distance h for $h/R = 2.25 \times 10^{-2}$ and 8.3% for $h/R = 4.75 \times 10^{-2}$. The stationary mode reported by Sirivat (1991) is observed with a stationary or a rotating cylindrical shroud.

As we saw in § 2.1, we can choose two other types of boundary conditions presented in figure 2. For the configuration with the radial gap $j_r/R = 7.14 \times 10^{-2}$ presented in figure 2(*a*) the sequence of transitions observed for $h/R > 1.96 \times 10^{-2}$ is very different from that described for the closed system, where the circular roll pattern was the first to be destabilized. However, Gauthier *et al.* (1998) observed the presence of circular rolls (CR) even with a rotating shroud. In our new geometry, we distinguished the development of only one instability, consisting of spiral rolls with $\varepsilon < 0°$ whose visualization is presented in figure 15. These structures are non-stationary, propagating with a radial component, and their phase velocity is positive.

On the other hand, in the case of a radial gap, the transition process observed for the smallest values of aspect ratio $h/R \leqslant 1.96 \times 10^{-2}$ is identical to that presented § 5.2 for the closed configuration.

The experiments with the configuration of figure 2(*b*) were carried out at $h/R = 14.29 \times 10^{-2}$, the axial gap being in this case 5% of the height. In this geometry, visualizations of the flow reveal a primary transition leading to a stationary system of spiral rolls defined by a positive angle ε (see figure 16). It is in the same type of geometry that Sirivat (1991) observed a stationary instability consisting of quasi-circular rolls.

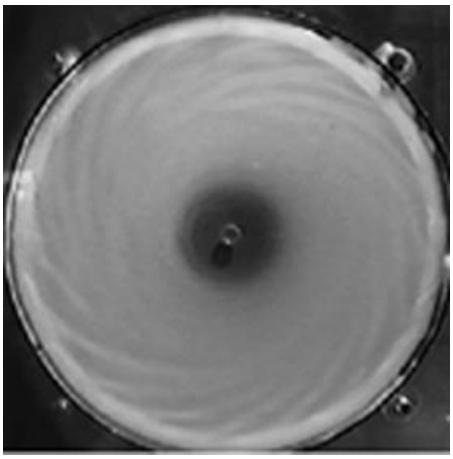

FIGURE 15. Geometry with radial gap: visualization of non-stationary rolls with $\varepsilon < 0°$ ($h/R = 11.43 \times 10^{-2}$, $Re = 11.1 \times 10^3$).

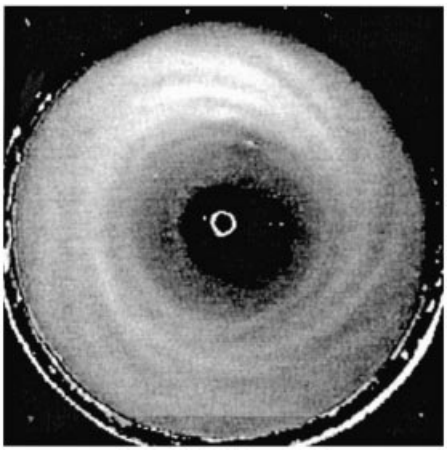

FIGURE 16. Geometry with axial gap: visualization of the stationary rolls with $\varepsilon > 0°$ ($h/R = 14.29 \times 10^{-2}$, $Re = 19.7 \times 10^3$).

The differences in the transition processes observed for these geometries with radial and axial gaps compared to those obtained for a closed configuration show the strong influence of the boundary conditions. But this influence seems to decrease when the aspect ratio decreases. Indeed, for small aspect ratios, we observed an identical sequence of transition for the closed configuration and for other configurations with a radial gap.

7. Concluding discussion

This systematic study enables us to construct the transition diagram (presented in figure 2) of the flow between a fixed and a rotating disk confined in a closed geometry, for a large range of the flow parameters h/R and Re. We have shown that this system presents various sequences of instabilities during its transition to turbulence according to the value of the aspect ratio. In the range explored, we

found three primary instabilities that affect the basic flow. When h/R is sufficiently small, the transition concerns a flow close to a pure shear with joined boundary layers (the torsional Couette flow). The primary bifurcation leads to the development of a network of spiral rolls (SRIII). Secondary instabilities lead at higher Reynolds numbers to the appearance of localized turbulent structures, which can be spots (SP) or solitary waves (SW). Turbulence occurs through the progressive invasion of these structures into the laminar flow. In contrast, for intermediate and large aspect ratios, the primary bifurcations result from the destabilization of flows where the viscous effects are confined to boundary layers in the vicinity of the disks. Spiral rolls (SRI and SRII) and circular rolls (CR) have been visualized and the transition to turbulence occurs by the interaction of these waves. Most of our observations are in agreement with previous experimental or numerical works.

Finally, let us mention the numerical work of Hoffmann *et al.* (1998) on the stability of the Ekman–Couette flow, which consists of a Couette flow with a superimposed rotation around an axis normal to the plates. When the rotation rate is increased, this evolves from a purely viscous flow to a separated boundary layer flow, as is the case for the rotating/stationary disk flow. As in the stability analysis of the Batchelor solution of the flow between a rotating and a stationary disk presented by San'kov & Smirnov (1992), Hoffmann *et al.* (1998) recovered the type 1 and 2 boundary layer instabilities (see § 1). Moreover, for purely viscous flow these two studies reveal the existence of a primary instability consisting of stationary (Hoffmann *et al.* 1998) or nearly stationary (San'kov & Smirnov 1992) rolls. These analyses can be compared to our own experimental results. This comparison was in fact already made in Hoffmann *et al.* (1998), where the similarity between the experimental and analytical transition diagrams is striking. More specifically, in the case of separated boundary layers, type 1 and type 2 instabilities as calculated by Hoffmann *et al.* (1998) would then correspond to modes III and IV (inward propagating waves) of San'kov & Smirnov (1992), and to SRI and CR structures of our own experimental study. Indeed both of these modes are localized in the Bödewadt layer and are characterized by $\varepsilon \approx 0^\circ$ for CR and by $\varepsilon > 0^\circ$ for RSI. For the merged boundary layer flow, the SRIII mode we observed would correspond to the stationary mode also obtained by the two analytical works. A more recent study by Hoffmann & Busse (2000) addresses the appearance of isolated solitary vortices in the Ekman–Couette flow. Such finite-amplitude vortex solutions have also been computed by Cherhabili & Ehrenstein (1995) for plane Couette flow. Although the inner structure of these isolated vortices is difficult to compare to the turbulent visual appearance of our solitary waves, it is noteworthy that the solutions of Hoffmann & Busse (2000) are obtained in a domain of the flow parameters which is comparable to ours. However it appears that this domain extends also to separated boundary layer flows which is not the case in our experiments where the solitary waves exist only as a tertiary regime of small aspect ratio flows.

Therefore, this experimental study presents for the first time the detailed transition diagram of the flow confined between a rotating and a stationary disk. It exhibits the great variety of instabilities and patterns associated with these rotating flows. In particular we identified two main routes of transition to turbulence: a sequence of supercritical bifurcations leads to wave turbulence for large separating gaps, unlike small aspect ratio values for which we observed the formation of localized turbulent structures characteristic of subcritical transitions and spatio-temporal intermittency.

We wish to thank L. Tuckerman for helpful comments.

REFERENCES

Balakumar, P. & Malik, M. R. 1990 Traveling disturbances in rotating-disk flow. *Theor. Comput. Fluid Dyn.* **2**, 125–137.

Batchelor, G. K. 1951 Note on a class of solutions of the Navier-Stokes equations representing steady rotationally-symmetric flow. *Q. J. Mech. Appl. Maths.* **4**, 29–41.

Bödewadt, U. T. 1940 Die Drehströmung über festem Grunde. *Z. Angew. Math. Mech.* **20**, 241–253.

Chauve, M. P. & Tavera, G. 1984 Rotating disk flow, transition to turbulence. In *Cellular Structures in Instabilities*. Lecture Notes in Physics, vol. 210 (ed. J. E. Wesfried & S. Zaleski), pp. 307–318. Springer.

Cherhabili, A. & Ehrenstein, U. 1995 Spatially localized two-dimensional finite-amplitude states in plane Couette flow. *Eur. J. Mech.* B/*Fluids* **14**, 677–696.

Cousin-Rittemard, N. 1996 Contribution à l'étude des instabilités des écoulements axisymétriques en cavité inter-disques de type rotor-stator. Thèse de Doctorat, Université Paris VI.

Cousin-Rittemard, N., Daube, O. & Le Quere, P. 1998 Sur la nature de la première bifurcation des écoulements interdisques. *C. R. Acad. Sci. Paris* IIb **326**, 359–366.

Daily, J. W. & Nece, R. E. 1960 Chamber dimension effects on induced flow and frictional resistance of enclosed rotating disks. *Trans. ASME: J. Basic Engng* **82**, 217–232.

Dauchot, O. & Daviaud, F. 1995 Finite-amplitude perturbation and spot growth mechanism in plane Couette flow. *Phys. Fluids* **4**, 335–343.

Daviaud, F., Hegseth, J. & Bergé, P. 1992 Subcritical transition to turbulence in plane Couette flow. *Phys. Rev. Lett.* **69**, 2511–2514.

Dijkstra, D. & Heijst, G. J. F. van 1983 The flow between two finite rotating disks enclosed by a cylinder. *J. Fluid Mech.* **128**, 123–154.

Ekman, V. W. 1905 On the influence of the Earth's rotation on ocean currents. *Arkiv. Mat. Astr. Fys.* **2** (11), 1–52.

Faller, A. J. 1963 An experimental study of the instability of the laminar Ekman boundary layer. *J. Fluid Mech.* **15**, 560–576.

Faller, A. J. 1991 Instability and transition of disturbed flow over a rotating disk. *J. Fluid Mech.* **230**, 245–269.

Faller, A. J. & Kaylor, R. E. 1966*a* Investigations of stability and transition in rotating boundary layers. In *Dynamics of Fluids and Plasmas* (ed. S. I. Pai *et al.*), pp. 309–329. Academic.

Faller, A. J. & Kaylor, R. E. 1966*b* A numerical study of the instability of the laminar Ekman boundary layer. *J. Atmos. Sci.* **23**, 466–480.

Fernandez-Feria, R. 2000 Axisymmetric instabilities of Bödewadt flow. *Phys. Fluids* **12**, 1730–1739.

Gauthier, G., Gondret, P. & Rabaud, M. 1998 Motions of anisotropic particles: Application to visualization of three-dimensional flow. *Phys. Fluids* **10**, 2147–2154.

Gauthier, G., Gondret, P. & Rabaud, M. 1999 Axisymmetric propagating vortices in the flow between a stationary and a rotating disk enclosed by a cylinder. *J. Fluid Mech.* **386**, 105–126.

Greenspan, H. P. 1968 *The Theory of Rotating Fluids*. Cambridge University Press.

Gregory, N., Stuart, J. T. & Walker, W. S. 1955 On the stability of three-dimensional boundary layers with application to the flow due to a rotating disk. *Phil. Trans. R. Soc. Lond.* A **248**, 155–199.

Hoffmann, N. & Busse, F. H. 2000 Isolated solitary vortex solutions for the Ekman-Couette layer. *Eur. J. Mech.* B/*Fluids* **19**, 391–402.

Hoffmann, N., Busse, F. H. & Chen, W.-L. 1998 Transitions to complex flows in the Ekman–Couette layer. *J. Fluid Mech.* **366**, 311–331.

Itoh, M. 1988 Instability and transition of the flow around a rotating disk in a casing. *Toyota Rep.* **36**, 28–36 (in Japanese).

Itoh, M. 1991 On the instability of flow between coaxial rotating disks. *Boundary Layer Stability and Transition to Turbulence*, ASME FED vol. 114, pp. 83–89.

Jarre, S., Le Gal, P. & Chauve, M. P. 1996 Experimental study of rotating disk flow instability. I. Natural flow. *Phys. Fluids* **8**, 496–508.

Kármán, T. von 1921 Uber laminare und turbulente Reibung. *Z. Angew. Math. Mech.* **1**, 233–252.

Kobayashi, R., Kohama, Y. & Takamadate, C. 1980 Spiral vortices in boundary layer transition regime on a rotating disk. *Acta Mech.* **35**, 79–82.

Lance, G. N. & Rogers, M. H. 1962 The axially symmetric flow of a viscous fluid between two infinite rotating disks. *Proc. R. Soc. Lond.* A **248**, 109–121.

Lilly, D. K. 1966 On the instability of Ekman boundary layer. *J. Atmos. Sci.* **23**, 481–494.

Lingwood, R. J. 1995 Absolute instability of the boundary layer on a rotating disk. *J. Fluid Mech.* **299**, 17–33.

Lingwood, R. J. 1996 An experimental study of absolute instability of the rotating-disk boundary-layer flow. *J. Fluid Mech.* **314**, 373–405.

Lingwood, R. J. 1997 Absolute instability of the Ekman layer and related rotating flows. *J. Fluid Mech.* **331**, 405–428.

Lopez, J. M. 1996 Flow between a stationary and a rotating disk shrouded by a co-rotating cylinder. *Phys. Fluids* **8**, 2605–2613.

Lopez, J. M. & Weidman, P. D. 1996 Stability of stationary endwall boundary layers during spin-down. *J. Fluid Mech.* **326**, 373–398.

Manneville, P. 1991 *Structures Dissipatives, Chaos et Turbulence*. Aléa, Saclay.

Owen, J. M. & Rogers, R. H. 1989 *Flow and Heat Transfer in Rotating-Disc Systems, Volume 1: Rotor-Stator Systems*. Research Studies Press, Taunton, UK.

Pikhtov, S. V. & Smirnov, E. M. 1993 Boundary layer stability on a rotating disk with corotation of the surrounding fluid. *Fluid. Dyn.* **27**, 657–663.

Rabaud, M. 1994 Visualisation de spirales dans un écoulement confiné entre disques tournants. *Compte Rendu de la Journée d'Etude du 23 Novembre 1994: Ecoulements et Convection dans les Machines Tournantes*. Société Française des Thermiciens.

Randriamampianina, A., Elena, L., Fontaine, J. P. & Schiestel, R. 1997 Numerical predictions of laminar, transitional and turbulent flows in shrouded rotor-stator systems. *Phys. Fluids* **9**, 1696–1713.

San'kov, P. I. & Smirnov, E. M. 1985 Bifurcation and transition to turbulence in the gap between rotating and stationary parallel disks. *Fluid. Dyn.* **19**, 695–702.

San'kov, P. I. & Smirnov, E. M. 1992 Stability of viscous flow between rotating and stationary disks. *Fluid. Dyn.* **26**, 857–864.

Savas, Ö. 1983 Circular waves on a stationary disk in rotating flow. *Phys. Fluids* **26**, 3445–3448.

Savas, Ö. 1985 On flow visualization using reflective flakes. *J. Fluid Mech.* **152**, 235–248.

Savas, Ö. 1987 Stability of Bödewadt flow. *J. Fluid Mech.* **183**, 77–94.

Schouveiler, L. 1998 Sur les instabilités des écoulements entre un disque fixe et un disque en rotation. Thèse de Doctorat, Université Aix-Marseille II.

Schouveiler, L., Le Gal, P. & Chauve, M.-P. 1998 Stability of a travelling roll system in a rotating disk flow. *Phys. Fluids* **10**, 2695–2697.

Schouveiler, L., Le Gal, P., Chauve, M.-P. & Takeda, Y. 1996 Experimental study of the stability of the flow between a rotating and a stationary disk. In *Advances in Turbulence VI* (ed. S. Gavrilakis *et al.*), pp. 385–388. Kluwer.

Schouveiler, L., Le Gal, P., Chauve, M.-P. & Takeda Y. 1999 Spiral and circular waves in the flow between a rotating and a stationary disk. *Exps. Fluids* **26**, 179–187.

Serre, E., Crespo Del Arco, E. & Bontoux, P. 2001 Annular and spiral patterns in a flow between a rotating and a stationary disk. *J. Fluid Mech.* **434**, 65–100.

Sirivat, A. 1991 Stability experiment of flow between a stationary and a rotating disk. *Phys. Fluids* A **3**, 2664–2671.

Smith, N. H. 1946 Exploratory investigation of laminar boundary layer oscillations on a rotating disk. *NACA Tech. Note* 1227.

Takeda, Y. 1986 Velocity profile measurement by ultrasound Doppler shift method. *Intl J. Heat Fluid Flow* **7**, 313–318.

Wilkinson, S. P. & Malik, M. R. 1983 Stability experiments in rotating-disk flow. *AIAA Paper* 83–1760.

Wimmer, M. 1978 Die zähe Strömung im Spalt zwischen einer rotierenden Scheibe und einem ruhenden Gehäuse. *Z. Angew. Math. Mech.* **58**, 350–353.

Zandbergen, P. J. & Dijkstra, D. 1987 Von Kármán swirling flows. *Ann. Rev. Fluid Mech.* **19**, 465–491.